Theoretical rationalization of the singlet-triplet gap in oleds materials: Impact of charge-transfer character

To be submitted to *J. Chem. Theory Comput.* (revised version)

Theoretical rationalization of the singlet-triplet gap in OLEDs materials: impact of charge-transfer character

M. Moral[1], L. Muccioli[2,3], W.-J. Son[4], Y. Olivier[5], and J. C. Sancho-García[1*]

[1] Departamento de Química Física, Universidad de Alicante, 03080 Alicante, Spain

[2] Department of Industrial Chemistry "Toso Montanari", University of Bologna, 40136, Italy

[3] Laboratoire de Chimie des Polymères Organiques, University of Bordeaux, 33607 Pessac, France

[4] Samsung Advanced Institute of Technology, Gyeonggi-do, 443-803, South Korea

[5] Laboratory for Chemistry of Novel Materials, University of Mons, 7000 Mons, Belgium

December 4, 2014

*E-mail: jc.sancho@ua.es

Abstract

New materials for OLED applications with low singlet-triplet energy splitting have been recently synthesized in order to allow for the conversion of triplet into singlet excitons (emitting light) via a Thermally Activated Delayed Fluorescence (TADF) process, which involves excited-states with a non-negligible amount of Charge-Transfer (CT). The accurate modeling of these states with Time-Dependent Density Functional Theory (TD-DFT), the most used method so far because of the favorable trade-off between accuracy and computational cost, is however particularly challenging. We carefully address this issue here by considering materials with small (high) singlet-triplet gap acting as emitter (host) in OLEDs, and by comparing the accuracy of TD-DFT and the corresponding Tamm-Dancoff Approximation (TDA), which is found to greatly reduce error bars with respect to experiments thanks to better estimates for the lowest singlet-triplet transition. Finally, we quantitatively correlate the singlet-triplet splitting values with the extent of CT, using for it a simple metric extracted from calculations with double-hybrid functionals, that might be applied in further molecular engineering studies.

1 Introduction

Organic semiconductors materials have been thoroughly used in the last decade for the development of a wide range of optoelectronic devices such as miniaturized organic field-effect transistors,[1–4] photovoltaic cells,[5–7] and

organic light-emitting diodes,[8–11] commonly known as OLEDs. One of the most rich subfields within last years, for the purpose of having brighter and more efficient OLEDs for massive electronics, has been the study of new organic semiconductors showing electroluminescence. These materials are classified according to the underlying mechanism for light emission: fluorescence or phosphorescence depending on the origin of the radiative decay (ie., if it is produced from a singlet or triplet excited states, respectively[12]) the latter yielding to phosphorescent-based OLEDs (PHOLEDs). The spin-statistics affects the formation of the exciton upon the electron-hole combination, see Figure 1, and that the radiative decay from triplet excitons (75 %) is spin-forbidden according to the selection rules. Thus, only singlet excitons (25 %) can emit light,[13] degrading efficiency and increasing power consumption. Initially, phosphorescent materials containing rare or transition metals[14–18] were proposed to act as emissive triplet states, mainly due to singlet-triplet combination via effective spin-orbit coupling interaction, relaxing the spin-forbiddennes of the electronic transition between ground singlet and triplet excited states (see Figure 1) and thus increasing the emission yield up to considerable efficiencies.[18,19] However, these PHOLEDs also have some known disadvantages such as a mineral extraction and toxicity issues concerning the contained metals,[20] and lower electroluminescence efficiency under high current density.[21] Moreover, although numerous efficient red and green light emitting materials have been obtained, blue or white PHOLEDs reliable enough for technological applications seem more hard to develop.[18,22]

For standard fluorescent materials, the 75 % of triplet excitons generated by due spin statistics is lost through non-radiative processes. Actually, up-conversion of dark triplet states to emissive singlet excitons can occur by

two mechanisms: Triplet-Triplet Annihilation (TTA or P-type delayed fluorescence) and Thermally-Activated Delayed Fluorescence (TADF or E-type delayed fluorescence). Indeed, it has recently demonstrated that the internal quantum efficiency (IQE) can potentially raise to 100 % by a thermally activated up-conversion of triplet into singlet states,[23–25] resulting in highly efficient OLEDs with no need for phosphorescent materials and the possibility of obtaining bright blue emitters, giving thus very high total singlet yields.[11,26] In the case of TTA, the triplet up-conversion could achieve efficiencies up to 37.5 %, because only one photon is emitted by every pair of annihilated triplet states, while all of triplet excitons can ideally be up-converted to singlet states in the case of TADF.[27] Note that the rate of the latter mechanism becomes high only when the energy gap between the lowest triplet and singlet states, ΔE^{ST}, is small (see also Figure 1). Recent studies show how this requirement can be met by molecules containing a sufficiently spatially separated Highest Occupied (HO) and Lowest Unoccupied (LU) Molecular Orbitals (MO).[28,29]

The computational estimate of ΔE^{ST} is challenging: the abundant literature for singlet-triplet splitting of OLEDs materials shows that for a given molecule theoretical predictions might differ up to tenths of eV, a quantity which is of the same order than the property itself. In order to advance the state-of-the-art of these calculations, here we aim at: (i) identifying and validating a method able to calculate as accurately as possible the singlet-triplet splitting of conjugated compounds; (ii) bracketing the influence of any technicality of the calculations in the final estimates, and then the weight of associated theoretical errors in further studies; and (iii) analyzing in detail the kind of excitation leading to the lowest singlet and triplet-excited states,

be them of a charge-transfer nature or not. Note that we are mainly interested here in the description of the processes briefly sketched in Figure 1, where the different (possible) emitting mechanisms from an organic molecule are displayed, and less in how the electron-hole pair is injected into the active layer or migrates across it.[30,31]

In this systematic study, we will thus focus on a set of compounds, selected from recent key references within the field,[32] whose chemical structure is presented in Figure 2. It comprises molecules with moderately high ($0.5 - 0.7$ eV) singlet-triplet energy splitting, such as phenylcarbazole (PhCz), triphenylamine (TPA), and 4,4'-bis(carbazol-9-yl)-*p*-biphenyl (pCBP), typically acting as the hole/electron transporting layer, as well as some with low ($0.1 - 0.3$ eV) singlet-triplet energy splitting, such as spiro-annulated triphenylamine/carbazole (ACRFLCN), 2-phenoxazine-4,6-diphenyl-1,3,5-triazine (PXZ-TRZ), and 4,5-di(9h-carbazol-9-yl)phthalonitrile (2CzPN), acting as guests/emitters; which can be considered as representative of TADF materials to be used in real devices.[33]

2 Computational details

We specify next a set of technical details for the sake of the complete reproducibility of the results. The ORCA 3.0.0 quantum-chemical package[34] was used for most all the calculations reported here, unless otherwise noticed, since for some complementary calculations we adopted the GAUSSIAN09 package;[35] we have employed mostly hybrid (eg. PBE0[36,37]) and double-hybrid (egs. B2-PLYP[38] and B2GP-PLYP[39]) density functionals. Note we are much more interested in providing insightful conclusions, and structure-

property guidelines for these materials, than in benchmarking of theoretical methods against large training sets; consequently, we have thus based our choice of functionals on previous benchmark studies of excited-state properties.

First, the numerical thresholds were systematically increased (TightSCF, TightOpt, Grid6, NoFinalGrid options in ORCA) with respect to defaults. Then, whenever possible, we use the 'resolution-of-the-identity' (RI) and 'chain-of-spheres' (COSX) techniques[40,41] leading to large speedup of the calculations without any lack of accuracy, which was particularly useful for the largest molecules treated here. For preliminary calculations, and for comparison with existing results in the literature, the moderate 6-31G* basis set was used. Then, the sufficiently large def2-TZVP basis set[42] was always fixed for quality results, with the corresponding auxiliary functions (def2-TZVP/JK and def2-TZVP/C) taken from the library hardwired in the ORCA code. Post-processing of the results was done with gOpenMol[43] or Gaussview.[44]

Note also that both gas-phase and solution values can always be obtained, the latter through the use of the implemented solvation models. **For that purpose, and according to the availability of the specific solvation models in the softwares used, we employ both the non-equilibrium Polarizable Continuum Model (PCM) using the integral equation formalism variant (IEF-PCM) when dealing with hybrid methods,[45,46] and the COnductor-like Screening MOdel (COSMO)[47–49] in the case of double-hybrid methods, and with the default technical parameters.**

Vertical excitation (absorption) energies from the ground-state ($\tilde{X}$ or commonly denoted as S_0) to the first lowest singlet- ($\tilde{A}$ or S_1) and triplet-excited state ($\tilde{a}$ or T_1) of the molecules selected are calculated as $E_{VA}(S_1) = E(S_1)//E(S_0) - E(S_0)$, or $E_{VA}(T_1) = E(T_1)//E(S_0) - E(S_0)$, where '$E(X)//E(S_0)$' refers to energies of the involved excited-states but calculated at the optimized geometry of the ground state; the vertical singlet-triplet splitting is correspondingly obtained as $\Delta E^{ST} = E_{VA}(S_1) - E_{VA}(T_1)$. These absorption energies are calculated within the linear-response TD-DFT approach.

Adiabatic excitation energies are achieved through the corresponding expressions $E_{00}(S_1) = E(S_1) - E(S_0)$, or $E_{00}(T_1) = E(T_1) - E(S_0)$, where the minima of the respective excited-states is now considered; being defined now as $\Delta E_{00}^{ST} = E_{00}(S_1) - E_{00}(T_1)$. Where the geometry of the T_1 state can be accessed through spin-relaxed open-shell calculations, optimizing the geometry for the S_1 state needs the use of the implemented TD-DFT gradients[50] at a non-negligible computational cost. We neglect differences in Zero-Point Vibrational Energies (ZPVE) between ground- and excited-states, ΔE^{ZPVE}, which are known to be small and rather independent on basis sets and functional issues, ranging around a value of $\Delta E^{\mathrm{ZPVE}} = 0.08 \pm 0.04$ eV.[51,52]

As a guide for comparison between experimental and calculated values, we will hereafter employ in the following the MAXimum deviation (MAX), the Mean Absolute Deviation (MAD) and the Root Mean-Squared Deviation (RMSD), defined as:

$$\mathrm{MAX} = max\left\{|x_i|\right\}, \tag{1}$$

$$\mathrm{MAD} = \frac{1}{n}\sum_{i}^{n}|x_i|, \tag{2}$$

$$\text{RMSD} \;=\; \sqrt{\frac{1}{n}\sum_{i}^{n}|x_i|^2}, \tag{3}$$

for which $x_i = \Omega_i^{\text{calculated}} - \Omega_i^{\text{reference}}$, being Ω the corresponding excitation energies, and $\Omega_i^{\text{reference}}$ the experimentally available values with i running over the set of molecules studied.

3 Results and discussion

3.1 The Tamm-Dancoff approximation

The Tamm-Dancoff Approximation (TDA)[53,54] is imposed for all calculations, which may result in some differences with respect to some previously (non-TDA) published values; this is expected to mainly affect triplet excitation energies in the right direction (*vide infra*). In the TD-DFT linear-response regime, the excitation ($\Omega_{\text{TD-DFT}} = E_m - E_0$) between excited- ($E_m$) and ground-state ($E_0$) energies arises from the solution of the non-Hermitian eigenvalue problem:[55]

$$\begin{bmatrix} \mathbf{A} & \mathbf{B} \\ \mathbf{B}^\star & \mathbf{A}^\star \end{bmatrix} \begin{bmatrix} \mathbf{X} \\ \mathbf{Y} \end{bmatrix} = \Omega_{\text{TD-DFT}} \begin{bmatrix} \mathbf{1} & \mathbf{0} \\ \mathbf{0} & \mathbf{-1} \end{bmatrix} \begin{bmatrix} \mathbf{X} \\ \mathbf{Y} \end{bmatrix}, \tag{4}$$

with $\mathbf{X}$ ($\mathbf{Y}$) the set of (de-)excitation amplitudes. In the following, we will denote occupied (unoccupied) orbitals as i, j (a, b); and w_{HF} the weight of the HF-like exchange term entering into the form of the exchange-correlation hybrid functional itself, $E_{xc}[\rho]$. The matrix elements of the orbital rotation Hessians matrices $\mathbf{A}$ and $\mathbf{B}$ are given, for a hybrid density functional in spin-restricted case, by:

$$A_{ia,jb} \;=\; \delta_{ij}\delta_{ab}(\epsilon_a - \epsilon_i) + 2(ia|jb) - \text{w}_{\text{HF}}(ij|ab) + (1 - \text{w}_{\text{HF}})\,(ia|\hat{f}_{xc}|jb), \tag{5}$$

$$B_{ia,jb} \;=\; 2(ia|bj) - \text{w}_{\text{HF}}(ib|aj) + (1 - \text{w}_{\text{HF}})\,(ia|\hat{f}_{xc}|bj), \tag{6}$$

being ϵ_i the eigenvalues of the corresponding Kohn-Sham eigenvectors ϕ_i, and ia a compound index corresponding to the single substitution $\phi_i \rightarrow \phi_a$. The meaning of the involved integrals is as follows: (i) $(ia|\hat{f}_{xc}|jb)$ is the integral $\iint \phi_i^\star(\mathbf{r})\phi_a(\mathbf{r})\hat{f}_{xc}(\mathbf{r},\mathbf{r}')\phi_j^\star(\mathbf{r}')\phi_b(\mathbf{r}')d\mathbf{r}d\mathbf{r}'$, with $\hat{f}_{xc} = \frac{\delta^2 E_{xc}[\rho]}{\delta\rho(\mathbf{r})\rho(\mathbf{r}')}$ being the exchange-correlation kernel (this integral gives the linear-response of the exchange-correlation functional); and (ii) $(ia|jb)$ has the most common form $\iint \phi_i^\star(\mathbf{r})\phi_a(\mathbf{r})\frac{1}{|\mathbf{r}-\mathbf{r}'|}\phi_j^\star(\mathbf{r}')\phi_b(\mathbf{r}')d\mathbf{r}d\mathbf{r}'$, and can be viewed as an exchange-type integral, $(ia|jb)^K$, or as a Coulomb-type integral, $(ij|ab)^C$.

By neglecting the occupied-unoccupied elements of the matrix, which corresponds to setting $\mathbf{B} = 0$ in the full TD-DFT equations, Eq. (4), one arrives to the Hermitian Tamm-Dancoff Approximation (TDA) to the problem:

$$\mathbf{AX} = \Omega_{\mathrm{TDA}}\mathbf{X}, \tag{7}$$

which is numerically simpler and (often) easier to interpret. Note how in the case of having excitations with substantial charge-transfer character, the product $\phi_i(\mathbf{r})\phi_a(\mathbf{r})$ tends to vanish, and then the equations (5)-(6) simplify to:

$$A_{ia,jb} = \delta_{ij}\delta_{ab}(\epsilon_a - \epsilon_i) - \mathrm{w}_{\mathrm{HF}}(ij|ab), \tag{8}$$

$$B_{ia,jb} \approx 0, \tag{9}$$

expecting in this case almost negligible differences between both full TD-DFT and TDA results.[56]

We have then closely investigated the effect of the Tamm-Dancoff approximation on ΔE^{ST}, with results for the selected compounds gathered in Table 1. We note that although experimental estimates[32] are based on rate

constants of prompt and delayed fluorescence (in toluene and at room temperature), and are thus more related with $E_{00}(T_1)$ and $E_{00}(S_1)$ values, which involve excited-state geometry relaxation, we want to first analyze here the (possible) effect of TDA on vertical transition energies and show later on that the effect of geometry relaxation is weak on ΔE^{ST} values.

Whereas the gas-phase theoretical values at the TD-PBE0/6-31G* level[32] produced differences (MAX, MAD, and RMSD for ΔE^{ST}) of 0.58, 0.21, and 0.28 eV, respectively, the corresponding TDA-PBE0/6-31G* calculations reduced all the metrics to 0.23, 0.13, and 0.16 eV, respectively. Interestingly, the impact of TDA on the $E_{VA}(S_1)$ values seems to be rather limited, with variations with respect to previous (non-TDA) values ranging between 0.03 (PXZ-TRZ) and 0.11 (ACRFLCN), while the $E_{VA}(T_1)$ values can be largely affected (up to 0.40 eV for PhCz) or remain almost unaffected (0.01 eV for PXZ-TRZ). This might signal the presence of dominant CT-type excitations for some compounds, as follows from Eqs. (8)-(9), and especially in the case of PXZ-TRZ (*vide infra*). Note also that we have verified that this behavior holds independently of functional choice (TDA-PBE0/6-31G* vs. TDA-B3LYP/6-31G*) or computational code (ORCA or GAUSSIAN09, respectively) employed. The TDA scheme has been also recently shown to be rather accurate in reproducing absorption and emission vibrational band shapes,[57] even when the sum rule affecting the oscillator strength distribution is not longer fulfilled,[58] and it has been simplified (sTDA) to pave the way towards calculations for large systems.[59–61]

3.2 Dispersion and basis sets effects

We study next if the improvement of ground-state geometries, by addressing intra-molecular dispersion (attractive) effects by the recently introduced DFT–D3(BJ) model,[62–64] as well as the use of large (def2-TZVP) basis sets, have some effect on vertical excitation energies. Although the term 'dispersion' is normally associated with long-range non-covalent interactions,[65] the effects taken into account here are better termed medium-range intra-molecular interactions and can not be (in principle) neglected even for medium-sized organic molecules.[66]

We analyze first if dispersion corrections and basis sets effects might have some impact on ground-state geometries. We note that the calculated TDA-PBE0/6-31G*//PBE0-D3(BJ)/6-31G* excitation energies do not appreciably differ from previous (dispersion-uncorrected) values: differences in MAX, MAD and RMSD values are found below 0.01 eV with respect to values reported in section 3.1 (for more details about the use of the –D3(BJ) correction for optimizing ground-state geometries see the Supporting Information). However, what instead seems to matter is the use of large basis sets, see Table 1, since the differences between TDA-PBE0/def2-TZVP//PBE0-D3(BJ)/def2-TZVP and TDA-PBE0/6-31G*//PBE0-D3(BJ)/6-31G* excitation energies are significant: (i) $E_{VA}(S_1)$ can vary up to $\pm$0.1 eV; (ii) the impact on $E_{VA}(T_1)$ is slightly smaller, differing up to $\pm$0.05 eV; and (iii) the consequence is a variation of ΔE^{ST} between 0.0 and 0.2 eV, always in the right direction since the employed metrics MAX, MAD and RMSD decrease now to 0.17, 0.10, and 0.12 eV, respectively. As a final test of the optimal basis set size, we have also employed for PhCz and TPA the very large def2-QZVP basis set: going from def2-TZVP to def2-QZVP decreases the ΔE^{ST}

only by −0.02 eV in both molecules; it thus seems that the def2-TZVP basis set can be considered as safely converged.

3.3 Adiabaticity effects

We compare next adiabatic excitation energies from the ground-state to the lowest singlet, $E_{00}(S_1)$, and triplet, $E_{00}(T_1)$, states. The experimental values are derived from the onset of absorption and emission spectra in cyclohexane at 300 K, and from the peak maximum of the phosphorescent spectra in toluene at 77 K, respectively.[32] The theoretical $E_{00}(S_1)$ adiabatic energy can in principle be obtained after optimizing the lowest singlet state at the TD-PBE0-D3(BJ)/def2-TZVP level. However, severe convergence problems precluded to obtain this energy for some of the molecules, independently on functional choice (eg. PBE and B3LYP sanity checks were also performed). On the other hand, the $E_{00}(T_1)$ adiabatic energy is accessed after optimizing the spin-unrestricted lowest triplet state at the PBE0-D3(BJ)/def2-TZVP level, which does not suffer from that convergence problem. All the available results are included in Table S1 (Supporting Information). Interestingly, for both $E_{00}(S_1)$ and $E_{00}(T_1)$ excitations, the error with respect to experimental results is always reduced compared with the previous case of vertical absorption energies, the $E_{00}(T_1)$ values for the molecules ACRFLCN, PXZ-TRZ, and 2CzPN are now in very close agreement with experimental results, resulting in MAD and RMSD values for $E_{00}(T_1)$ of 0.10 and 0.06 eV, respectively.

3.4 Solvent embedding

The impact that solvation has on excitation energies is approximately described by using a dielectric continuum model, with the dielectric constant ($\epsilon_s = 2.4$) corresponding to the solvent (toluene) used in experiments for extracting the singlet-triplet gap. The use of a solvation model appears to be reasonably adequate in this case: the dielectric response originates mainly from electronic polarization thanks to the approximation relationship $\frac{n^2-1}{\epsilon_s-1} \approx 90$ %, with n the refractive index of the solvent taken here as $n = 1.5$, leaving thus only a small fraction from reorientation of the dipole moments of both molecule and solvent.

We have analyzed first the impact of solvation on the adiabatic energies for triplet states using the COSMO model. As a matter of illustration, the $E_{00}(T_1)$ values vary as much as 0.1 eV (e.g. PXZ-TRZ) resulting now in MAD and RMSD values for this energy of 0.13 and 0.07 eV, respectively, for the whole set. These values might be further corrected by dropping off spin-contamination[67] without any significant difference: MAD and RMSD values are now 0.12 and 0.06 eV, respectively, to be compared with values (former section) of 0.10 and 0.06 eV.

The values of $E_{VA}(T_1)$ also remains largely unaffected in solvent-phase; however, we have found a strong variation of the first singlet-excited state for molecules ACRFLCN, PXZ-TRZ, and 2CzPN using this solvent model. In particular, in the case of PXZ-TRZ, a dramatic overstabilization of its $E_{VA}(S_1)$ energy by up to -1.0 eV compared to experimental results[32] is obtained. This variation needs to be compared against a moderate solvatochromic shift of -0.04, -0.03, and -0.11 eV for PhCz, TPA, and pCBP,

respectively. These results seem to confirm again the marked charge-transfer character of the lowest singlet-singlet excitation for the former set of molecules, which calls for further investigation. Note that this behavior renders the value of ΔE^{ST} calculated with COSMO meaningless for ACRFLCN, PXZ-TRZ and 2CzPN molecules, requiring thus another theoretical choice if a balanced description of standard and charge-transfer singlet-singlet excitations needs to be achieved.

This prompts us to use next the **non-equilibrium** Polarizable Continuum Model (PCM) with the default technical parameters, for inferring both the $E_{VA}(S_1)$ and $E_{VA}(T_1)$ values (see Table 1). **In the non-equilibrium limit, there is a fast response of electrons of the solvent to the new configuration of the solute, and it is thus better adapted to vertical transition energies.** Considering now these results, a moderate solvatochromic shift between -0.02 and -0.07 eV is always found with respect to gas-phase, without suffering neither the pronounced overstabilization found before, and leading thus to very accurate metrics: MAD and RMSD values are now 0.11 and 0.13 eV, respectively. **It turned out that there is a significant interplay between the solvation model used and the way in which a functional is able to describe a charge-transfer excitation or not, or in other words, the kind of functional selected for these cases.**[68]

4 Charge-transfer excitations and associated metrics

4.1 On the use of double-hybrid density functionals

The high degree of specialization reached by density functionals of all kinds (the functional zoo) has not yet been fully translated to a more accurate description of excited-states, with PBE0 still being by far the favoured choice.[69–71] In the case of charge-transfer excitations, one could better use modern range-separated hybrid functional such as ωB97X.[72] However, since one deals here with intramolecular charge-transfer excitations, the $E_{VA}(S_1)$ values are systematically overestimated by around $0.8 - 0.9$ eV with this functional, in agreement with previous studies.[32] This result clearly reveals how difficult is to tackle efficiently the separation between medium- and long-range effects and its influence on excited-states properties.

However, the irruption of double-hybrid methods, after their pioneering implementation for use within the TD-DFT framework,[73] might lead to a good compromise in this case; note that the very few benchmarking studies performed up to now, exclusively for singlet-singlet energies, seems to confirm this prospect.[74–78] This is why we combine next the use of these functionals with some orbital-based metrics, to disclose first existing charge-transfer excitations and then fully characterize the relationships between these excitations and corresponding low singlet-triplet energy splittings.

We therefore start by analyzing the dependence of the results (singlet-singlet excitation energies: $E_{VA}(S_1)$) on the double-hybrid functional choice. For the case of PhCz, for which it seems clearly established the presence of an absorption maximum peaking at around 3.67 eV[79] almost independent of

solvent effects, we have compared the output of some Double-Hybrid (DH) expressions[80–82] in several flavors (B2-PLYP, B2GP-PLYP, B2π-PLYP, and PBE0-DH, see Table S2 in the Supporting Information) using toluene as solvent for the COSMO module. Whereas the TDA-PBE0/def2-TZVP//PBE0-D3(BJ)/def2-TZVP method (starting point) gives a value of 4.09 eV for this molecule, the use of B2-PLYP slightly improves it to 3.98 eV, with the other methods providing values roughly above it, and this trend holds for TPA and pCBP molecules too. However, for molecules with an envisioned large charge-transfer character, such as ACRFLCN, PXZ-TRZ or 2CzPN, it has been recognized before that a correct description of long-range charge-transfer excited states require non-local exchange[83] and/or correlation[77] kernel. Therefore, it might be interesting to consider functionals having large weights for these non-local exchange (ie. exact-like) and correlation (ie. perturbative-like) terms for comparison purposes. Table S2 shows the composition of several double-hybrid methods initially chosen, being therefore B2GP-PLYP the one fitting better (having $w_{EXX} = 0.65$ and $w_{PT2} = 0.36$) to the previous argument. We will thus restrict in the following to the discussion of the B2-PLYP and B2GP-PLYP results. **Due to this feature, and invoking again the large interplay between solvent models and the use of a (double-)hybrid functional,[68]** we obtain very decent metrics (MAD and RMSD) of 0.34 and 0.39 eV (for B2-PLYP) and 0.28 and 0.32 eV (for B2GP-PLYP) over the whole sef of compounds. One can argue that this accuracy metrics hardly shows the benefit of using a more costly DH functional instead of the standard PBE0 model. However, for the set of compounds with (expectedly) larger charge-transfer character, such as ACRFLCN, PXZ-TRZ or 2CzPN, the metrics (MAD and RMSD) are 0.16 and 0.20 eV (for B2GP-PLYP) compared to 0.25 and 0.25 eV for PBE0. We will thus adopt the B2GP-PLYP

model in the remainder of the study.

Note that for a double-hybrid functional the final $\Omega^{\mathrm{DH}}_{\mathrm{TDA}}$ values, gathered in Table 2, are obtained in a two-step fashion,

$$\Omega^{\mathrm{DH}}_{\mathrm{TDA}} = \Omega^{\mathrm{GH}}_{\mathrm{TDA}} + \mathrm{w}_{\mathrm{PT2}}\Delta^{(\mathrm{D})}, \tag{10}$$

where the perturbative-like correction[84] $\Delta^{(\mathrm{D})}$ is weighted by the $\mathrm{w}_{\mathrm{PT2}}$ value, and then added to the initial excitation energies ($\Omega^{\mathrm{GH}}_{\mathrm{TDA}}$) obtained for a standard (global) hybrid. All the eigenvectors and eigenvalues needed are obtained after converging self-consistently the Kohn-Sham equations for the corresponding global hybrid. Interestingly, for the chosen case of the B2GP-PLYP functional, the size of this correction is around -0.6 eV for PhCz, TPA, and pCBP molecules, but it is substantially larger for those molecules with charge-transfer excitations, between -0.8 eV for 2CzPN and -1.3 eV for ACRFLCN. This shows how the $\Delta^{(\mathrm{D})}$ correction must to be always included, having otherwise only the value provided by a hybrid functional weighted by the $\mathrm{w}_{\mathrm{EXX}}$ in Table S2, which might overestimate the experimental results according to their large weight ($\mathrm{w}_{\mathrm{EXX}} \geq 0.5$ normally in double-hybrid functionals[82]). The oscillator strengths (f) provided by both methods are also included in Table 2, although these must be regarded only for qualitative purposes[85] since the f-sum rule, also known as the Thomas-Reiche-Kuhn sum rule, which states that the sum of the f values of absorption transitions minus the sum of the f values of the emission transitions equals the number of electrons involved in the specific transition, is not longer fulfilled.

4.2 Natural Transition Orbitals and associated metrics

Additionally to the aforesaid features, the understanding of the way in which a TD-DFT calculation describes an electronically excited state can be hampered, especially in the case of having a marked charge-transfer character, by a large set of non-zero coefficients κ_{ia} quantifying the promotion from an occupied orbital (ϕ_i) to an unoccupied one (ϕ_a) to the excitation energy. This often makes a straightforward interpretation of the results difficult, due to the large number of determinants defining the excited-state, each one with its own amplitude κ_{ia}. However, one can find a more compact representation of the contribution that each electron-hole pair makes to the final excited state, as well as a set of orbitals with a meaning other than be used as intermediates to build the electronic density of the ground state, by resorting to the use of Natural Transition Orbitals (NTO),[86] ϕ'_i and ϕ'_a, which arise after diagonalization of the single-particle transition density matrix $\mathbf{T}$ having as elements:

$$T_{ia} = \sum_{\sigma} \langle \Psi_{\tilde{A}} | c^{\dagger}_{i\sigma} c_{a\sigma} | \Psi_{\tilde{X}} \rangle, \tag{11}$$

with σ a spin index. This transformation does not change the corresponding (accurate) excitation energies obtained before. We adopt here this procedure at the TDA-B2GP-PLYP/def2-TZVP//PBE0-D3(BJ)/def2-TZVP level, with the COSMO solvation model too, to analyze in depth the transition processes leading to the first singlet excited-state of the studied systems. Table 3 gathers the key information needed to characterize the nature and type of the excited-states found, including the values for the new set of coefficients λ_{ia} dominating the transition. All the excitations can be characterized now of a truly $\pi \rightarrow \pi^{\star}$ (HOMO to LUMO) nature, with these frontier orbitals asymmetrically distributed between the different parts of the molecule in the case of the charge-transfer compounds (eg. PXZ-TRZ) or spread out over the

whole molecular backbone (eg. PhCz), as depicted in Figure 3 for both cases.

From these orbitals, we can quantify the topology and extent of the electron-hole distance[87–91] by means of the following recently proposed index:[92,93]

$$\Delta\mathbf{r}(\mathrm{NTO}) = \frac{\sum_{ia} \lambda_{ia}^2 |\langle \phi'_a | \hat{\mathbf{r}} | \phi'_a \rangle - \langle \phi'_i | \hat{\mathbf{r}} | \phi'_i \rangle|}{\sum_{ia} \lambda_{ia}^2}, \tag{12}$$

where $\phi'_{i(a)}$ refers now to the new set of occupied (virtual) NTO, with λ_{ia} the corresponding coefficients for the involved excitation. Note also that a cutoff, $\Delta\mathbf{r}(\mathrm{NTO}) > 1.5 - 2.0$ Å, has been proposed before to distinguish, and then characterize, a charge-transfer excitation. We can immediately observe in Table 3 how $\Delta\mathbf{r}$(NTO) allows to clearly split the set of molecules into two subsets, those having low (pronounced) charge-transfer character: PhCz, TPA, and pCBP (ACRFLCN, PXZ-TRZ, 2CzPN), with two of them being especially prone to it (ACRFLCN and PXZ-TRZ) having as twice as value of the above cutoff. This quantitative results are in perfect agreement with the findings observed through previous sections, and helps to rationalize the performance of the different theoretical methods used along this study.

To further rationalize this feature, we explicitly write the singlet and triplet solution of the TD-DFT equations for the simplest two-level case as starting point:[94] One deals here with a single-electron excitation from frontier occupied to virtual orbitals (a $\phi_i \rightarrow \phi_a$ transition) and neglects all other interactions between occupied and/or virtual orbitals. Hence, the square roots of the corresponding eigenvalues problem:[56]

$$\mathbf{M} = \begin{bmatrix} \mathbf{A} & \mathbf{B} \\ \mathbf{B}^\star & \mathbf{A}^\star \end{bmatrix} = \begin{bmatrix} M_{ia\sigma,ia\sigma} & M_{ia\sigma,ia\tau} \\ M_{ia\tau,ia\sigma} & M_{ia\tau,ia\tau} \end{bmatrix} = \begin{bmatrix} \Delta\epsilon\,(\Delta\epsilon + 2K_{\uparrow,\uparrow}) & 2\Delta\epsilon K_{\uparrow,\downarrow} \\ 2\Delta\epsilon K_{\downarrow,\uparrow} & \Delta\epsilon\,(\Delta\epsilon + 2K_{\uparrow,\uparrow}) \end{bmatrix} \tag{13}$$

give the singlet and triplet excitation energies, respectively:

$$\Omega_S = \sqrt{\Delta\epsilon\left[\Delta\epsilon + 2\left(K_{\uparrow,\uparrow} + K_{\uparrow,\downarrow}\right)\right]}, \quad (14)$$

$$\Omega_T = \sqrt{\Delta\epsilon\left[\Delta\epsilon + 2\left(K_{\uparrow,\uparrow} - K_{\uparrow,\downarrow}\right)\right]}, \quad (15)$$

with $\Delta\epsilon = \epsilon_a - \epsilon_i$, and $K_{ia\sigma,ia\tau}$ depending on the two-electron integrals introduced above, $(ia|\hat{f}_{xc}^{\sigma,\tau}|ia)$ and $(ia|ia)$, with σ and τ spin-indices. These two roots further reduce in the TDA treatment to simply:

$$\Omega_S = \Delta\epsilon + K_{\uparrow,\uparrow} + K_{\uparrow,\downarrow}, \quad (16)$$

$$\Omega_T = \Delta\epsilon + K_{\uparrow,\uparrow} - K_{\uparrow,\downarrow}, \quad (17)$$

which can also be viewed as a linearization of the solutions one would obtain from the full TD-DFT equations (14)-(15). These two solutions are explicitly written as:

$$\Omega_S = \Delta\epsilon + (HL|\hat{f}_{xc}^{\uparrow,\uparrow}|HL) + (HL|f_{xc}^{\uparrow,\downarrow}|HL) + 2(HL|HL), \quad (18)$$

$$\Omega_T = \Delta\epsilon + (HL|f_{xc}^{\uparrow,\uparrow}|HL) - (HL|\hat{f}_{xc}^{\uparrow,\downarrow}|HL), \quad (19)$$

with H and L refer now to the HOMO and LUMO orbitals involved in the (two-level) excitation, and $\Delta\epsilon$ the corresponding eigenvalue difference. This gives an expression for $\Delta E^{ST} = \Omega_S - \Omega_T = 2K_{\uparrow,\downarrow} = 2(HL|HL) + 2(HL|\hat{f}_{xc}^{\uparrow,\downarrow}|HL)$. It can be clearly seen now that for having a low ΔE^{ST} values one needs a low overlap between the involved orbitals, ie. the product $\phi_H(\mathbf{r})\phi_L(\mathbf{r})$ would have to asymptotically vanish as it happens for instance for the PXZ-TRZ molecule (see Figure 3).

Briefly, the computational design concept followed is to decrease the singlet-triplet splitting by allowing spatial separation (the larger the better) of the electron-hole pair upon excitation (the so-called donor-acceptor

approach[28]) although, however, a minimal overlap should be guaranteed between the frontier orbitals involved in the transitions to the excited state in order to allow for effective emission and non-vanishing oscillator strengths. The large correlation found between the (experimental) singlet-triplet splittings and the (calculated) values of $\Delta\mathbf{r}$(NTO) is presented in Figure 4, showing a correlation coefficient of 0.95 for the fitting to a function $A_0/\left(A_1 + \Delta\mathbf{r}(\text{NTO})\right)$, with $A_0 = 1.13$ eV Å and $A_1 = 1.56$ eV. The function selected intends to represent the screened and shifted Coulomb interaction between the quasi-particles involved in the excitation, accounting also for some of its physical limits: when $\Delta\mathbf{r}(\text{NTO}) \to 0$ ($\Delta\mathbf{r}(\text{NTO}) \to \infty$) then $\Delta E^{ST} \to 0.7$ eV ($\Delta E^{ST} \to 0.0$ eV). Thereby, a large intra-molecular charge-transfer character of the S_0 to S_1 excitation would lead to very low singlet-triplet energy separation. Actually, we can predict a value of $\Delta\mathbf{r}(\text{NTO}) \approx 4$ Å for having a singlet-triplet splitting as low as 0.2 eV. Interestingly, the Supporting Information also includes the results using the TDA-PBE0/def2-TZVP method instead of the TDA-B2GP-PLYP/def2-TZVP one and, owing to the similar trend found, the former also emerges as a promising and cheap alternative.

5 Conclusions

We have explored in this work the performance of the linear-response Tamm-Dancoff approximation to the prediction of singlet-triplet energy differences (ΔE^{ST}) for a set of compounds with OLED applications.[95] This energy gap is known to be a very sensitive property depending on the charge-transfer nature of the underlying excitations.[96] Our results reveal that: (i) the geometry of the ground-state can be safely obtained at the PBE0-D3(BJ)/def2-TZVP level, including large basis sets (def2-TZVP) and dis-

persion corrections –D3(BJ); (ii) the Tamm-Dancoff approximation is key to reduce significantly the error for $E_{VA}(T_1)$ energies, while the corresponding $E_{VA}(S_1)$ values remain almost unaffected; this error decrease still continues with the use of large basis sets leading to the TDA-PBE0/def2-TZVP//PBE0-D3(BJ)/def2-TZVP recommended model chemistry for a clear compromise between accuracy and computational cost; (iii) the use of double-hybrid density functionals within the linear-response Tamm-Dancoff approach, thus at the TDA-B2GP-PLYP/def2-TZVP//PBE0-D3(BJ)/def2-TZVP level and for $E_{VA}(S_1)$ excitation energies, can also be considered to double-check the values of these transitions being charge-transfer or not; (iv) the use of natural transition orbitals, which are based on the electron-hole separation upon excitation, calculated with any of the two methods assessed, appears well suited for the quantitative description of the nature of the excitations in these compounds; and (v) the triplet excitation seems to be much more localized than the singlet one, the latter being thus more prone to charge-transfer related issues, an observation confirmed by the calculated distance between the centroids of the involved natural transition orbitals. Furthermore, we have found a strong inverse correlation between this distance and the ΔE^{ST} values, which might help to the computational design of new molecules with low energy separation between the lowest singlet and triplet excited states, and could be thus used in the development of new blue-emitting devices through the TADF mechanism.

Acknowledgements

This work was partially supported by the Samsung Advanced Institute of Technology (SAIT)'s Global Research Outreach (GRO) Program. In ad-

dition, the research in Bordeaux has been funded by the French State grant ANR-10-LABX-0042-AMADEus managed by the French National Research Agency under the initiative of excellence IdEx Bordeaux program (reference nANR-10-IDEX-0003-02) and the work in Mons was supported by the "Programme d'Excellence de la Région Wallonne" (OPTI2MAT project) and FNRS-FRFC.

Associated content

The Supporting Information contains: (i) a discussion about the influence of the -D3(BJ) dispersion correction for optimizing the ground-state geometries of the compounds; (ii) a remind note about the *triplet instability problem*; (iii) the results for the charge-transfer metrics (Figure S1) selected but from the set of NTO obtained at the PBE0/def2-TZVP level; (iv) the calculated (Table S1) adiabatic singlet and triplet energies; and (v) the detailed composition (Table S2) of the double-hybrid density functionals used along the work. This information is available free of charge via the Internet at http://pubs.acs.org/.

References

1. Horowitz, G. *Adv. Mater.* **1998**, *10*, 365.

2. Zaumseil, J.; Sirringhaus, H. *Chem. Rev.* **2007**, *107*, 1296.

3. Bürgi, L.; Turbiez, M.; Pfeiffer, R.; Bienewald, F.; Kirner, H.-J.; Winnewisser, C. *Adv. Mater.* **2008**, *20*, 221.

4. Lee, J.; Han, A.-R.; Yu, H.; Shin, T.J.; Yang, C.; Oh, J.-H. *J. Am. Chem. Soc.* **2013**, *135*, 9540.

5. Sakamoto, Y.; Suzuki, T.; Kobayashi, M.; Gao, Y.; Fukai, Y.; Inoue, Y.; Sato, F.; Tokito, S. *J. Am. Chem. Soc.* **2004**, *126*, 8138.

6. Tang, M.L.; Reichardt, A.D.; Miyaki, N.; Stoltenberg, R.M. *J. Am. Chem. Soc.* **2008**, *130*, 6064.

7. Otón, F.; Pfattner, R.; Pavlica, E.; Olivier, Y.; Moreno, E.; Puigdollers, J.; Bratina, G.; Cornil, J.; Fontrodona, X.; Más-Torrent, M.; Veciana, J.; Rovira, C. *Chem. Mat.* **2011**, *23*, 851.

8. *Organic Light-Emitting Devices*; Müllen, K., Scherf, U., Eds.; Wiley-VCH Verlag GmbH & Co. KGaA: New York, 2006.

9. Endo, A.; Sato, K.; Yoshimura, K.; Kai, T.; Kawada, A.; Miyazaki, H.; Adachi, C. *App. Phys. Lett.* **2011**, *98*, 083302.

10. Nakagawa, T.; Ku, S.-Y.; Wong, K.-T.; Adachi, C. *Chem. Comm.* **2012**, *48*, 9580.

11. Zhang, Q.; Li, J.; Shizu, K.; Huang, S.; Hirata, S.; Miyazaki, H.; Adachi, C. *J. Am. Chem. Soc.* **2012**, *101*, 09306.

12. Sato, K.; Shizu, K.; Yoshimura, K.; Kawada, A.; Miyazaki, H.; Adachi, C. *Phys. Rev. Lett.* **2013**, *110*, 247401.

13. Uoyama, H.; Goushi, K.; Shizu, K.; Nomura, H.; Adachi, C. *Nature* **2012**, *492*, 234.

14. Adachi, C.; Baldo, M.A.; Thompson, M.E.; Forrest, S.R. *J. Appl. Phys.* **2011**, *90*, 5048.

15. O'Brien, D.F.; Baldo, M.A.; Thompson, M.E.; Forrest, S.R. *Appl. Phys. Rev.* **2009**, *74*, 442.

16. Fernández-Hernández, J.M.; Yang, C.H.; Beltrán, J.; Lemaur, V.; Polo, F.; Frölich, R.; Cornil, J.; De Cola, L. *J. Am. Chem. Soc.* **2011**, *133*, 10543.

17. Fernández-Hernández, J.M.; Beltrán, J.; Lemaur, V.; Gávez-López, M.D.; Chien, C.H.; Polo, F.; Orselli, E.; Fröhlich, R.; Cornil, J.; De Cola, L. *Inorg. Chem.* **2013**, *52*, 1812.

18. Chen, X.L.; Yu, R.; Zhang, Q.-K.; Zhou, L.-J.; Wu, X.-Y.; Zhang, Q.; Lu, C.-Z. *Chem. Mater.* **2013**, *25*, 3910.

19. Dias, F.B.; Bourdakos, K.N.; Jankus, V.; Moss, K.C.; Kamtekar, K.T.; Bhalla, V.; Santos, J.; Bruyce, M.R.; Monkman, A.P. *Adv. Mater.* **2013**, *25*, 3707.

20. *Giant Metallic Deposits*; Laznicka, P.; Springer-Verlag: Heidelberg, 2006.

21. Baldo, M.A.; Adachi, C.; Forrest, S.R. *Phys. Rev. B.* **2000**, *62*, 10967.

22. Méhes, G.; Nomura, H.; Zhang, Q.; Nakagawa, T.; Adachi, C. *Angew. Chem. Int. Ed.* **2012**, *51*, 11311.

23. Brown, C.T.; Kondakov, D.J. *J. Soc. Inf. Disp.* **2004**, *12*, 323.

24. Kondakov, D.; Pawlik, T.D.; Hatwer, T.K.; Spindler, J.P. *J. Appl. Phys.* **2009**, *106*, 124510.

25. Endo, A.; Ogasawara, M.; Takahashi, A.; Yokoyama, D.; Kato, Y.; Adachi, C. *Adv. Mater.* **2009**, *21*, 4802.

26. Goushi, K.; Yoshida, K.; Sato, K.; Adachi, C. *Nat. Photonics* **2012**, *6*, 253.

27. Serevičius, T.; Nakagawa, T.; Kuo, M.-C.; Cheng, S.-H.; Wong, K.-T.; Chang, C.-H.; Kwong, R.C.; Xia, S.; Adachi, C. *Phys. Chem. Chem. Phys.* **2013**, *15*, 15850.

28. Milián-Medina, B.; Gierschner, J. *Org. Electron.* **2012**, *13*, 985.

29. Tao, Y.; Yuan, K.; Chen, T.; Xu, P.; Li, H.; Chen, R.; Zheng, C.; Zhang, L.; Huang, W. DOI: 10.1002/adma.201402532

30. Coropceanu, V.; Cornil, J.; da Silva Filho, D.A.; Olivier, Y.; Silbey, R.; Brédas, J.-L. *Chem. Rev.* **2007**, *107*, 926.

31. Cornil, J.; Verlaak, S.; Martinelli, N.; Mityashin, A.; Olivier, Y.; Van Regemorter, T.; Muccioli, L.; Zannoni, C.; Castet, F.; Beljonne, D.; Heremans, P. *Acc. Chem. Res.* **2013**, *46*, 434.

32. Huang, S.; Zhang, Q.; Shiota, Y.; Nakagawa, T.; Kuwabara, K.; Yoshizawa, K.; Adachi, C. *J. Chem. Theory Comput.* **2013**, *9*, 3872.

33. Adachi, C. *Jpn. J. Appl. Phys.* **2014**, *53*, 060101.

34. Neese, F.; *WIREs Comput. Mol. Sci.* **2012**, *2*, 73.

35. Frisch, M.J.; Trucks, G.W.; Schlegel, H.B.; Scuseria, G.E.; Robb, M.A.; Cheeseman, J.R.; Scalmani, G.; Barone, V.; Mennucci, B.; Petersson, G.A.; Nakatsuji, H.; Caricato, M.; Li, X.; Hratchian, H.P.; Izmaylov, A.F.; Bloino, J.; Zheng, G.; Sonnenberg, J.L.; Hada, M.; Ehara, M.; Toyota, K.; Fukuda, R.; Hasegawa, J.; Ishida, M.; Nakajima, T.; Honda, Y.; Kitao, O.; Nakai, H.; Vreven, T.; Montgomery, J.A., Jr.; Peralta, J.E.; Ogliaro, F.; Bearpark, M.; Heyd, J.J.; Brothers, E.; Kudin, K.N.; Staroverov, V.N.; Kobayashi, R.; Normand, J.; Raghavachari, K.; Rendell, A.; Burant, J.C.; Iyengar, S.S.; Tomasi, J.; Cossi, M.; Rega, N.; Mil-

lam, M.J.; Klene, M.; Knox, J.E.; Cross, J.B.; Bakken, V.; Adamo, C.; Jaramillo, J.; Gomperts, R.; Stratmann, R.E.; Yazyev, O.; Austin, A.J.; Cammi, R.; Pomelli, C.; Ochterski, J.W.; Martin, R.L.; Morokuma, K.; Zakrzewski, V. G.; Voth, G.A.; Salvador, P.; Dannenberg, J.J.; Dapprich, S.; Daniels, A.D.; Farkas, Ö.; Foresman, J.B.; Ortiz, J.V.; Cioslowski, J.; Fox, D.J. *Gaussian 09*, Revision C.01; Gaussian, Inc.: Wallingford CT, 2009.

36. Perdew, J.P.; Ernzerhof, M.; Burke, K. *J. Chem. Phys.* **1996**, *105*, 9982.

37. Adamo, C.; Barone, V. *J. Chem. Phys.* **1999**, *110*, 6158.

38. Grimme, S.; *J. Chem. Phys.* **2006**, *124*, 034108.

39. Karton, A.; Tarnopolsky, A.; Lamère, J.-F.; Schatz, G.C.; Martin, J.M.L. *J. Phys. Chem. A* **2008**, *112*, 12868.

40. Neese, F. *J. Comp. Chem.* **2003**, *24*, 1740.

41. Neese, F.; Wennmohs, F.; Hansen, A.; Becker, U. *Chem. Phys.* **2009**, *356*, 98.

42. Weigend, F.; Ahlrichs, R. *Phys. Chem. Chem. Phys.* **2005**, *7*, 3297.

43. Laaksonen, L. *J. Mol. Graph.* **1992**, *10*, 33.

44. Dennington, R.; Keith, T.; Millam, J.; *GaussView*, Version 5; Semichem Inc.: Shawnee Mission KS, 2009.

45. Tomasi, J.; Mennucci, B.; Cammi, R. *Chem. Rev.* **2005**, *105*, 2999.

46. Scalmani, G.; Frisch, M.J. *J. Chem. Phys.* **2010**, *132*, 114110.

47. Klamt, A.; Schürmann, G. *J. Chem. Soc. Perkin Trans.* **1993**, *2*, 799.

48. Andzelm, J.; Kömel, C.; Klamt, A. *J. Chem. Phys.* **1995**, *103*, 9312.

49. Sinnecker, S.; Rajendran, A.; Klamt, A.; Diedenhofen, M.; Neese, F. *J. Phys. Chem A* **2006**, *110*, 2235.

50. Petrenko, T.; Kossmann, S.; Neese, F. *J. Chem. Phys.* **2011**, *134*, 054116.

51. Laurent, A.D.; Jacquemin, D. *Int. J. Quantum Chem.* **2013**, *113*, 2019.

52. Fang, C.; Oruganti, B.; Durbeej, B. *J. Phys. Chem. A* **2014**, *118*, 4157.

53. Grimme, S. *Chem. Phys. Lett.* **1996**, *259*, 128.

54. Hirata, S.; Head-Gordon, M. *Chem. Phys. Lett.* **1999**, *314*, 291.

55. *Computational Quantum Chemistry*; McDouall, J.J.W.; RSC Publishing: Cambridge, 2013.

56. Casida, M.E.; Gutierrez, F.; Guan, J.; Gadea, F.-X.; Salahub, D.; Daudey, J.-P. *J. Chem. Phys.* **2000**, *113*, 7062.

57. Chantzis, A.; Laurent, A.D.; Adamo, C.; Jacquemin, D. *J. Chem. Theory Comput.* **2013**, *9*, 4517.

58. Huix-Rotllant, M.; Natarajan, B.; Ipatov, A.; Wawire, C.M.; Deutsch, T.; Casida, M. *Phys. Chem. Chem. Phys.* **2010**, *12*, 12811.

59. Grimme, S. *J. Chem. Phys.* **2013**, *138*, 244104.

60. Risthaus, T.; Hansen, A.; Grimme, S. *Phys. Chem. Chem. Phys.* **2014**, *16*, 14408.

61. Bannwarth, C.; Grimme, S. *Comput. Theor. Chem.* **2014**, *1040-1041*, 45.

62. Becke, A.D.; Johnson, E.R. *J. Chem. Phys.* **2005**, *122*, 154101.

63. Grimme, S.; Antony, J.; Ehrlich, S.; Krieg, H. *J. Chem. Phys.* **2010**, *132*, 154104.

64. Grimme, S.; Ehrlich, S.; Goerigk, L. *J. Comput. Chem.* **2011**, *32*, 1456.

65. Grimme, S. *WIREs Comput. Mol. Sci.* **2011**, *1*, 211.

66. Grimme, S.; Steinmetz, M. *Phys. Chem. Chem. Phys.* **2013**, *15*, 16031.

67. Rivero, P.; Jiménez-Hoyos, C.A.; Scuseria, G.E. *J. Phys. Chem. A* **2013**, *117*, 8073.

68. Chibani, S.; Charaf-Eddin, A.; Le Guennic, B.; Jacquemin, D. *J. Chem. Theory Comput.* **2013**, *9*, 3127.

69. Jacquemin, D.; Perpète, E.A.; Ciofini, I.; Adamo, C. *Acc. Chem. Res.* **2009**, *42*, 326.

70. Jacquemin, D.; Mennucci, B.; Adamo, C. *Phys. Chem. Chem. Phys.* **2011**, *13*, 16987.

71. Bousquet, D.; Fukuda, R.; Jacquemin, D.; Ciofini, I.; Adamo, C.; Ehara, M. *J. Chem. Theory Comput.* **2014**, *10*, 3969.

72. Chai, J.-D.; Head-Gordon, M. *Phys. Chem. Chem. Phys.* **2008**, *10*, 6615.

73. Grimme, S.; Neese, F. *J. Chem. Phys.* **2007**, *127*, 154116.

74. Goerigk, L.; Moellmann, J.; Grimme, S. *Phys. Chem. Chem. Phys.* **2009**, *11*, 4611.

75. Goerigk, L.; Grimme, S. *J. Chem. Phys.* **2010**, *132*, 184103.

76. Goerigk, L.; Grimme, S. *J. Chem. Theory Comput.* **2011**, *7*, 3272.

77. Di Meo, F.; Trouillas, P.; Adamo, C.; Sancho-García, J.C. *J. Chem. Phys.* **2013**, *139*, 164104.

78. Kozuch, S.; Martin, J.M.L. *J. Comput. Chem.* **2013**, *34*, 2327.

79. Sarkar, A.; Chakravorti, S. *J. Lumin.* **1998**, *78*, 205.

80. Sancho-García, J.C.; Pérez-Jiménez, A.J. *J. Chem. Phys.* **2009**, *131*, 084108.

81. Brémond, E.; Adamo, C. *J. Chem. Phys.* **2011**, *135*, 024106.

82. Sancho-García, J.C.; Adamo, C. *Phys. Chem. Chem. Phys.* **2013**, *15*, 14581.

83. Dreuw, A.; Weisman, J.L.; Head-Gordon, M. *J. Chem. Phys.* **2003**, *119*, 2943.

84. Head-Gordon, M.; Rico, R.J.; Oumi, M.; Lee, T.J. *Chem. Phys. Lett.* **1994**, *219*, 21.

85. Grüning, M.; Marini, A.; Gonze, X. *Nano Lett.* **2009**, *9*, 2820.

86. Martin, R.L. *J. Chem. Phys.* **2003**, *118*, 4775.

87. Peach, M.J.G.; Benfield, P.; Helgaker, T.; Tozer, D.J. *Mol. Phys.* **2008**, *128*, 044118.

88. Le Bahers, T.; Adamo, C.; Ciofini, I. *J. Chem. Theory Comput.* **2011**, *7*, 2498.

89. Ciofini, I.; Le Bahers, T.; Adamo, C.; Odobel, F.; Jacquemin, D. *J. Phys. Chem. C* **2012**, *116*, 11946.

90. Etienne, T.; Assfeld, X.; Monari, A. *J. Chem. Theory Comput.* **2014**, *10*, 3896.

91. Etienne, T.; Assfeld, X.; Monari, A. *J. Chem. Theory Comput.* **2014**, *10*, 3906.

92. Guido, C.A.; Cortona, P.; Mennucci, B.; Adamo, C. *J. Chem. Theory Comput.* **2013**, *9*, 3118.

93. Guido, C.A.; Cortona, P.; Adamo, C. *J. Chem. Phys.* **2014**, *140*, 104101.

94. Cordova, F.; Doriol, L.J.; Ipatov, A.; Casida, M.; Filippi, C.; Vela, A. *J. Chem. Phys.* **2007**, *127*, 164111.

95. Brunner, K.; van Dijken, A.; Börner, H.; Bastiaansen, J.J.A.M.; Kiggen, N.M.M.; Langeveld, B.M.W. *J. Am. Chem. Soc.* **2004**, *126*, 6035.

96. Dreuw, A.; Head-Gordon, M. *Chem. Rev.* **2005**, *105*, 4009.

- **Table 1.** Calculated $E_{VA}(S_1)$ and $E_{VA}(T_1)$ values (in eV) and corresponding energy difference ΔE^{ST}. The experimental values for the latter property are also included, as well as the MAX and RMSD (in eV) values with respect to them.

- **Table 2.** Calculated $E_{VA}(S_1)$ values (in eV) and oscillator strenghts (between parentheses) for B2-PLYP and B2GP-PLYP methods. The experimental $E_{VA}(S_1)$ values (in eV) are also included.

- **Table 3.** Description, at the TDA-B2GP-PLYP/def2-TZVP//PBE0-D3(BJ)/def2-TZVP level, of the lowest singlet-singlet excitation process (from occupied ϕ'_i to unoccupied ϕ'_a) by using NTO and corresponding occupation number λ_{ia} (the threshold for printing occupation numbers is fixed at 0.02), as well as resulting $\Delta\mathbf{r}$(NTO) (in Å) values.

Table 1:

	Molecule:	PhCz	TPA	pCBP	ACRFLCN	PXZ-TRZ	2CzPN	MAX	RMSD
TD-DFT[a]	$E_{VA}(S_1)$	4.141	4.063	3.717	2.717	2.314	2.992		
	$E_{VA}(T_1)$	3.059	3.098	2.892	2.556	2.269	2.530		
	ΔE^{ST}	1.08	0.96	0.82	0.16	0.04	0.46	0.53	0.28
TDA[b]	$E_{VA}(S_1)$	4.233	4.092	3.761	2.828	2.349	3.066		
	$E_{VA}(T_1)$	3.457	3.386	3.190	2.819	2.279	2.696		
	ΔE^{ST}	0.78	0.71	0.57	0.01	0.07	0.37	0.23	0.16
TDA[c]	$E_{VA}(S_1)$	4.129	3.921	3.731	2.989	2.334	3.077		
	$E_{VA}(T_1)$	3.412	3.411	3.153	2.916	2.322	2.719		
	ΔE^{ST}	0.72	0.51	0.58	0.07	0.01	0.36	0.17	0.12
TDA[d]	$E_{VA}(S_1)$	4.083	3.837	3.740	2.828	2.416	2.991		
	$E_{VA}(T_1)$	3.394	3.332	3.200	2.818	2.380	2.668		
	ΔE^{ST}	0.69	0.51	0.54	0.01	0.04	0.32	0.23	0.13
Exp. values	ΔE^{ST}	0.55	0.57	0.71	0.24	0.06	0.31		

[a] Calculated at the TD-PBE0/6-31G*//B3LYP/6-31G* level (taken from Ref.[32]).
[b] Calculated here at the TDA-PBE0/6-31G*//PBE0/6-31G* level.
[c] Calculated here at the TDA-PBE0/def2-TZVP//PBE0-D3(BJ)/def2-TZVP level.
[d] Calculated here at the TDA-PBE0/def2-TZVP//PBE0-D3(BJ)/def2-TZVP level, and with the PCM module for the solvent (toluene).

Table 2:

	Molecule:	PhCz	TPA	pCBP	ACRFLCN	PXZ-TRZ	2CzPN
TDA[a]	B2-PLYP	3.978	3.948	3.913	2.612	2.061	2.870
		(0.042)	(0.031)	(1.072)	(0.001)	(0.003)	(0.104)
	B2GP-PLYP	4.150	4.130	4.176	2.962	2.396	3.145
		(0.047)	(0.034)	(1.193)	(0.002)	(0.005)	(0.126)
	Exp. values	3.66	3.74	3.80	3.05	2.73	3.19

[a] Calculated here at the TDA-B2(GP)-PLYP/def2-TZVP//PBE0-D3(BJ)/def2-TZVP level, and with the COSMO module for the solvent (toluene).

Table 3:

Molecule	ϕ'_i	ϕ'_a	λ_{ia}	$\Delta\mathbf{r}$(NTO)
PhCz	HOMO	LUMO	0.816	0.60
	(H-1)OMO	(L+1)UMO	0.141	
TPA	HOMO	LUMO	0.879	0.14
	(H-1)OMO	(L+1)UMO	0.036	
	(H-2)OMO	(L+2)UMO	0.030	
pCBP	HOMO	LUMO	0.804	0.25
	(H-1)OMO	(L+1)UMO	0.133	
ACRFLCN	HOMO	LUMO	0.986	3.75
PXZ-TRZ	HOMO	LUMO	0.996	4.98
2CzPN	HOMO	LUMO	0.936	2.57
	(H-1)OMO	(L+1)UMO	0.048	

- **Figure 1.** Sketch of an energy diagram showing the main light emitting processes for the organic materials of interest for OLEDs applications.

- **Figure 2.** Chemical structure of the investigated compounds. The hydrogen atoms and corresponding C–H bonds have been omitted for clarity.

- **Figure 3.** Isocontour plots of the calculated HOMO (left) and LUMO (right) Natural Transition Orbitals for the PhCz (top) and PXZ-TRZ (bottom) molecules. The size and colour describe the amplitude and sign, respectively, of the lobes of orbitals.

- **Figure 4.** Dependence of the experimental singlet-triplet splitting on the calculated electron-hole distance ($\Delta\mathbf{r}$(NTO)), at the TDA-B2GP-PLYP/def2-TZVP//PBE0-D3(BJ)/def2-TZVP level, in the S_1 state for the set of molecules investigated. The dashed line represents the fitting function $A_0/\left(A_1 + \Delta\mathbf{r}(\mathrm{NTO})\right)$, with the value and units of the parameters specified in the text.

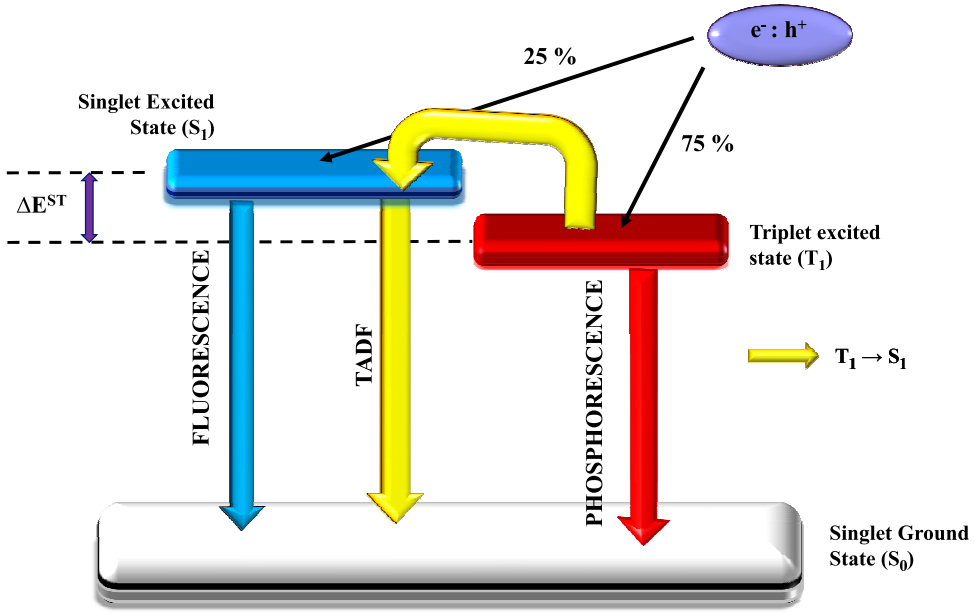
e⁻ : h⁺
25 %
75 %
Singlet Excited
State (S1)
ΔEST
Triplet excited
state (T1)
FLUORESCENCE
TADF
PHOSPHORESCENCE
T1 → S1
Singlet Ground
State (S0)

Figure 1.

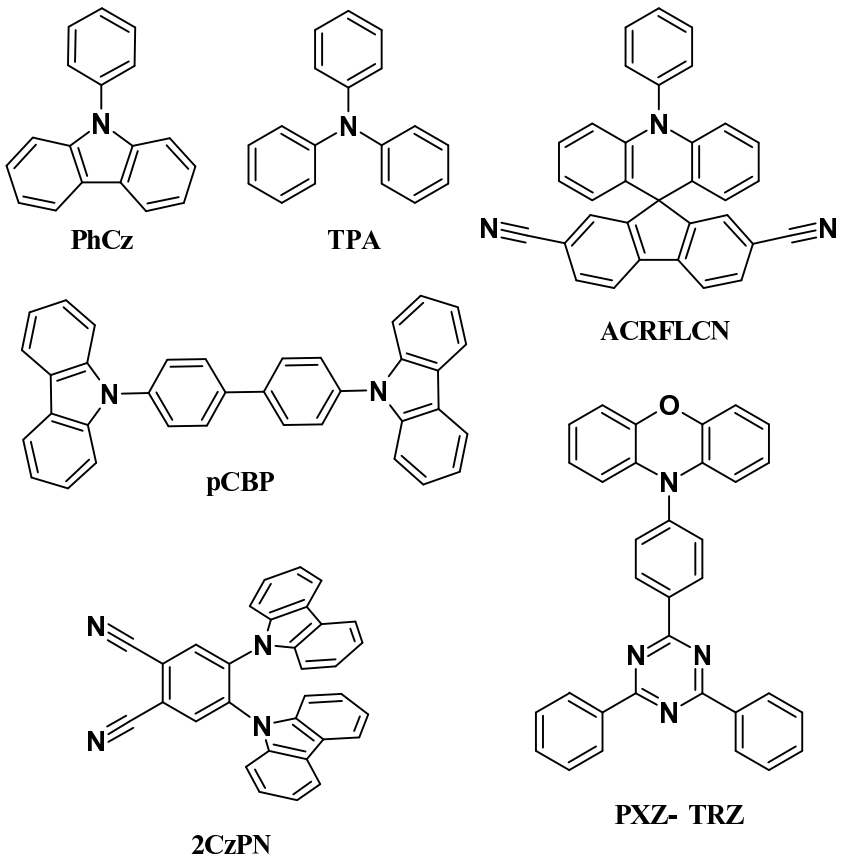

Figure 2.

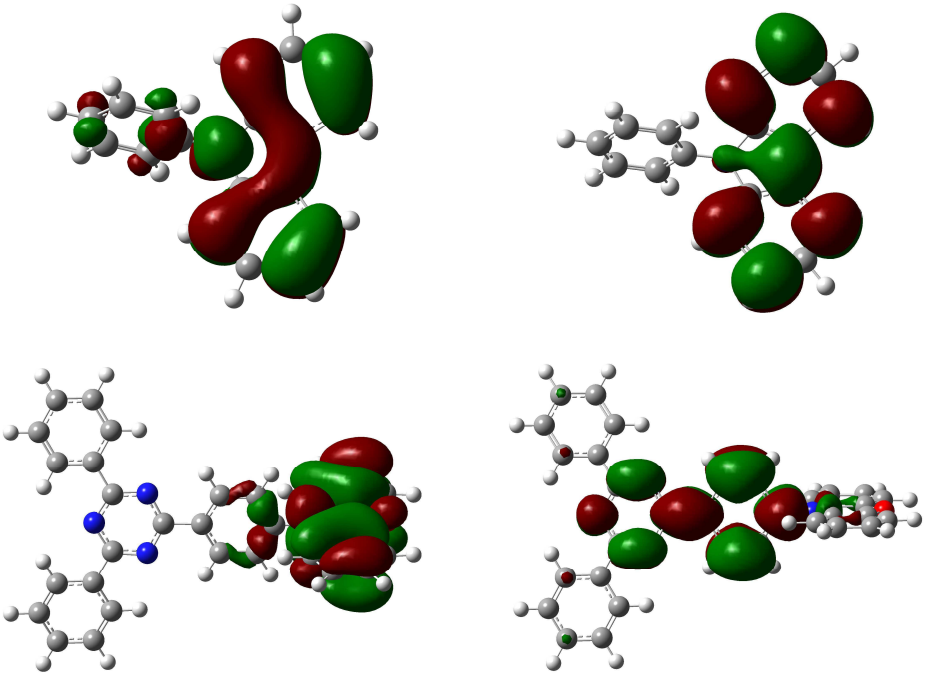

Figure 3.

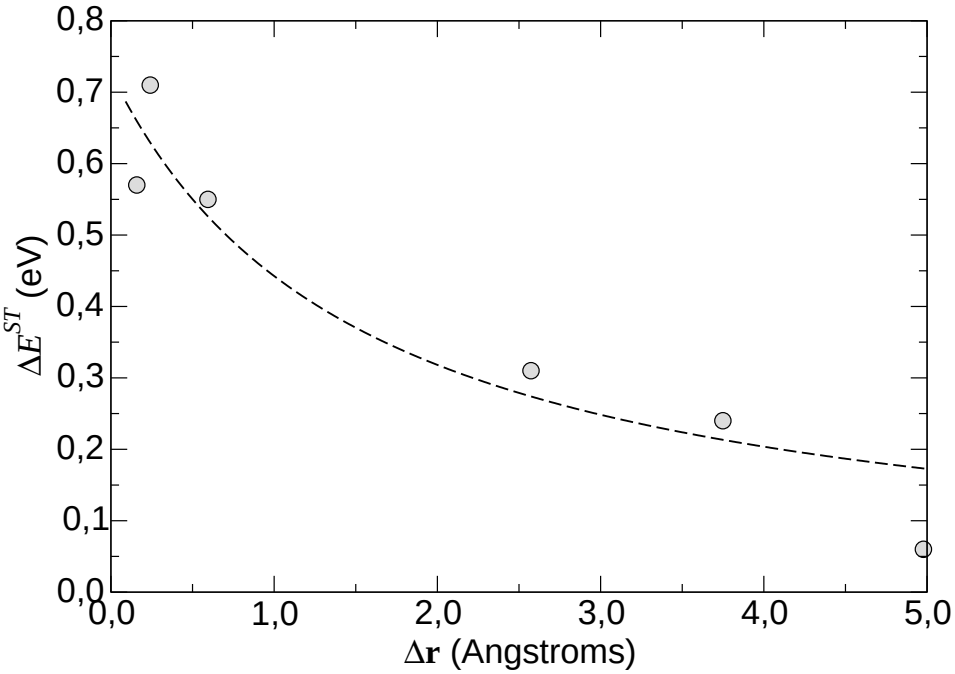
0,8
0,7
0,6
0,5
0,4
0,3
0,2
0,1
0,0
ΔE^{ST} (eV)
0,0
1,0
2,0
3,0
4,0
5,0
$\Delta \mathbf{r}$ (Angstroms)

Figure 4.